Journal of the European Ceramic Society 20 (2000) 2743–2751

www.elsevier.com/locate/jeurceramsoc

The microstructures, magnetic properties and impedance analysis of Mn–Zn ferrites doped with B_2O_3

J. Fan *, F.R. Sale

Manchester Materials Science Centre, University of Manchester and UMIST, Grosvenor Street, Manchester M1 7HS, UK

Abstract

The relationship between the microstructure, magnetic properties and impedance spectroscopy of Mn–Zn ferrites doped with B_2O_3 (up to 0.5 wt.%) has been further investigated. The ferrites were prepared by using a citrate gel processing route. A uniform microstructure with relatively small grains (9.6±0.7 μm) is observed for undoped ferrites (boron-free), which enables good magnetic properties to be achieved (initial permeability μ_i is 2400, power loss P_L is 26.3 kW/m^3 at 100 mT).The results on the samples doped with B_2O_3 show that the doping does not benefit the magnetic properties of these gel-derived ferrites, but it promotes grain growth significantly. Discontinuous grain growth at low doping levels (<0.2 wt.%) results in poor magnetic properties. A maximum value of the initial permeability (μ_i: ~2600) and a second minimum value (37.2 kW/m^3 at 100 mT) in power loss are obtained at the 0.25 wt.% B_2O_3 doping level when the sample has a relatively uniform microstructure with larger grain size (39.5±3.3 μm). With further increases in B_2O_3 doping ($\geqslant 0.5$ wt.%), the increased porosity and presence of a B-rich phase result in deteriorated magnetic properties. The results of impedance measurement are closely related to the changes in the microstructure which result from these B_2O_3 additions. By using two models for impedance measurement analysis (The Koops' model and the simple model), the contributions of B_2O_3 to grain boundary resistivity and bulk resistivity can be separated. It is shown that, whilst B_2O_3 has previously been considered to act as only a grain boundary additive, the impedance analysis indicates that both boundary resistivity and grain (bulk) resistivity are increased, thus implying the possible solution of some B_2O_3 within the ferrite spinel structure or an effective change in composition of grain as result of presence of B_2O_3 at the grain boundaries.

Keywords: Mn–Zn ferrites; Gel processing; B_2O_3 doping; Discontinuous grain growth; Magnetic property; Impedance analysis

1. Introduction

Manganese–zinc ferrites are used widely in telecommunications and related applications. The extrinsic properties of Mn–Zn ferrites, such as the initial permeability and magnetic loss, can be influenced strongly by doping with small amount of additives.[1,2] Therefore, numerous studies on the effect of the additives to Mn–Zn ferrites have been carried out. Among the various additives, boron oxide is known as a sintering aid, which has the similar effects to SiO_2.[3–5] An early investigation conducted by Fan and Sale[6] suggested that B_2O_3 doping does not benefit the magnetic properties of pure Mn–Zn ferrites, but promotes grain growth significantly.

The microstructure changes associated with the use of doping additives also bring about changes in the resistivities of ferrites. The electrical resistivities of soft ferrites are important as high resistivity can reduce eddy current losses which become increasingly important as the operating frequency is raised. The additions may either substitute within the spinel ferrite, and so alter the bulk resistivity, or they may segregate to grain boundaries, and so alter the grain boundary resistivities. Impedance analysis measurements may allow the contributions of additives to grain boundary resistivity and bulk resistivity to be separated with the result that such the impedance analysis can be used to provide more information on the role of boron doping.

To understand the true influence of small amounts of additives, it must be ensured that chemical homogeneity is obtained in the specimens. In recent years, several specialised chemical preparation techniques have been used for powder preparation to yield chemically homogeneous powder, such as coprecipitation,[7] wet methods employing aqueous solutions[8,9] and various gel techniques.[10–12] Of these, the citrate gel method is attractive because of its comparative simplicity and high chemical

* Corresponding author.

0955-2219/00/$ - see front matter
PII: S0955-2219(00)00230-2

homogeneity of product. Hence it has been widely used in the investigations on the effects of small amounts of additives in electrical and magnetic ceramics, such as superconductors,[12] ZnO varistors,[13] and soft ferrites.[14–17]

As mentioned above, to further clarify the effect of B_2O_3 doping on Mn–Zn ferrites, a systemic study was necessary. In a previous preliminary investigation,[6] it shows that the most significant B_2O_3 doping levels are between 0 and 0.5 wt.%. Based on this range of doping levels, this paper presents the effects of B_2O_3 on the microstructure, resistivity and magnetic properties of Mn–Zn ferrites, and focuses on the relationship between microstructure changes and the impedance analysis. All of the specimens were prepared via the citrate gel processing route.

2. Experimental

2.1. Preparation of ferrite powders

Analytical grade citric acid and nitrates of manganese, zinc and iron in the required proportions to give a nominal composition of $Mn_{0.57}Zn_{0.35}Fe_{2.08}O_4$ were each dissolved in deionised water, then mixed together to produce the solution for gel processing. The amount of citric acid used was that necessary to bind the metal ions if all the NO_3 ions were replaced. H_3BO_3 (99.5% pure) was used as boron additive, which was also dissolved in the mixed solutions to give the different B_2O_3 doping levels (0, 0.1, 0.15, 0.2, 0.25, 0.5 wt.%). The mixed solutions were concentrated using a rotary evaporator at 75±5°C to give the viscous gels, which then were dried in a vacuum oven at 80±5°C for 12 h. To form ferrite powders, the dried precursors were heated for 2 h at 300°C and then a further 2 h at 700°C. The resultant powders were deagglomerated by ball milling for 6 h in the polyurethane bottles with low carbon steel balls and deionised water, then dried at 105±5°C for 12 h. Granules were obtained by passing the dried powders through a screen of nominal 0.3 mm opening.

2.2. Preparation of samples

Pellets (10 mm in diameter, 3 mm in height) and toroids (25 mm in outside diameter, 18 mm in inside diameter and 3 mm in height) were pressed by a single action uniaxial press at 80 MPa. The samples were sintered at 1300°C for 2 h in air with a heating rate of 150°C/h and cooled in nitrogen with a cooling rate of 150°C/h. The sintered densities of samples were determined using Archimedes method. Typically, 3–5 samples were measured to obtained the experiment data. The theoretical density is taken as 5.12 g/cm^3, which is calculated from the formulation and the lattice parameters.

2.3. Microstructural studies

Microstructures of the sintered samples were examined using optical and scanning electron microscope (Philips 505 with an energy dispersive X-ray analytical facility EDAX). The average grain size was determined on the photomicrographs using Mendelson's intercept method.[18]

2.4. Magnetic properties

The magnetic inductances of the sintered toroids were measured at 10 kHz at room temperature using a Hewlett–Packard LCR meter (4284A). The values of initial permeability (μ_i) were obtained from the inductance data. The magnetic losses (total power loss, P_L) of the toroids with 10 primary and 10 secondary windings were determined at frequencies of 16, 32, 64 and 128 kHz and a flux density of 100 mT at 20°C using a laboratory built B–H loop and magnetic loss measuring system, in which the temperature rise of the toroids was controlled by immersion within a silicone oil bath.

2.5. Impedance analysis

A Solartron 1260 impedance analyser was used for the impedance analysis. The measurements were conducted at room temperature. The grain boundary resistance and bulk resistance were determined from the intercepts of the complex-impedance dispersion curve with the real impedance (Z') axis.

3. Results and discussion

3.1. Sintered density, microstructure and grain growth

Fig. 1 shows the sintered densities of samples. It can be seen that the density slightly increased with the

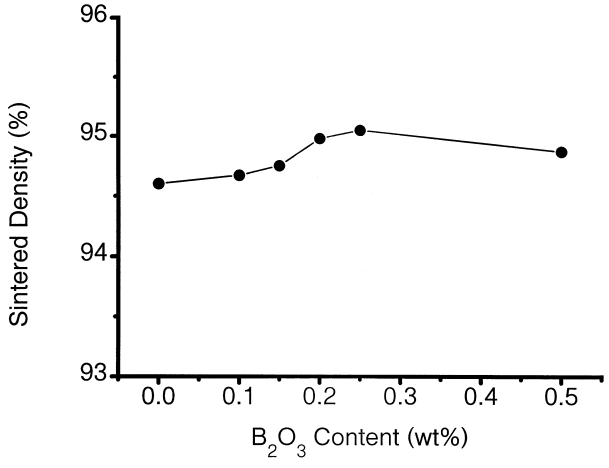

Fig. 1. The relationship between sintered density and the B_2O_3 content.

addition of small amounts of B_2O_3 up to 0.25 wt.%. Further increases in the doping level give decreases in the density. Fig. 2 shows the typical optical micrographs of the samples. The undoped sample (Fig. 2a, B_2O_3-free) has a uniform microstructure with fairly small grains. These small grains are nearly pore-free, and the average grain size is 9.6±0.7 μm. With B_2O_3 doping, a duplex structure showing discontinuous grain growth was observed at the low doping levels (< 0.2 wt.%) (Fig. 2b, 0.1 wt.% and 2c, 0.15 wt.%). At the 0.25 wt.%

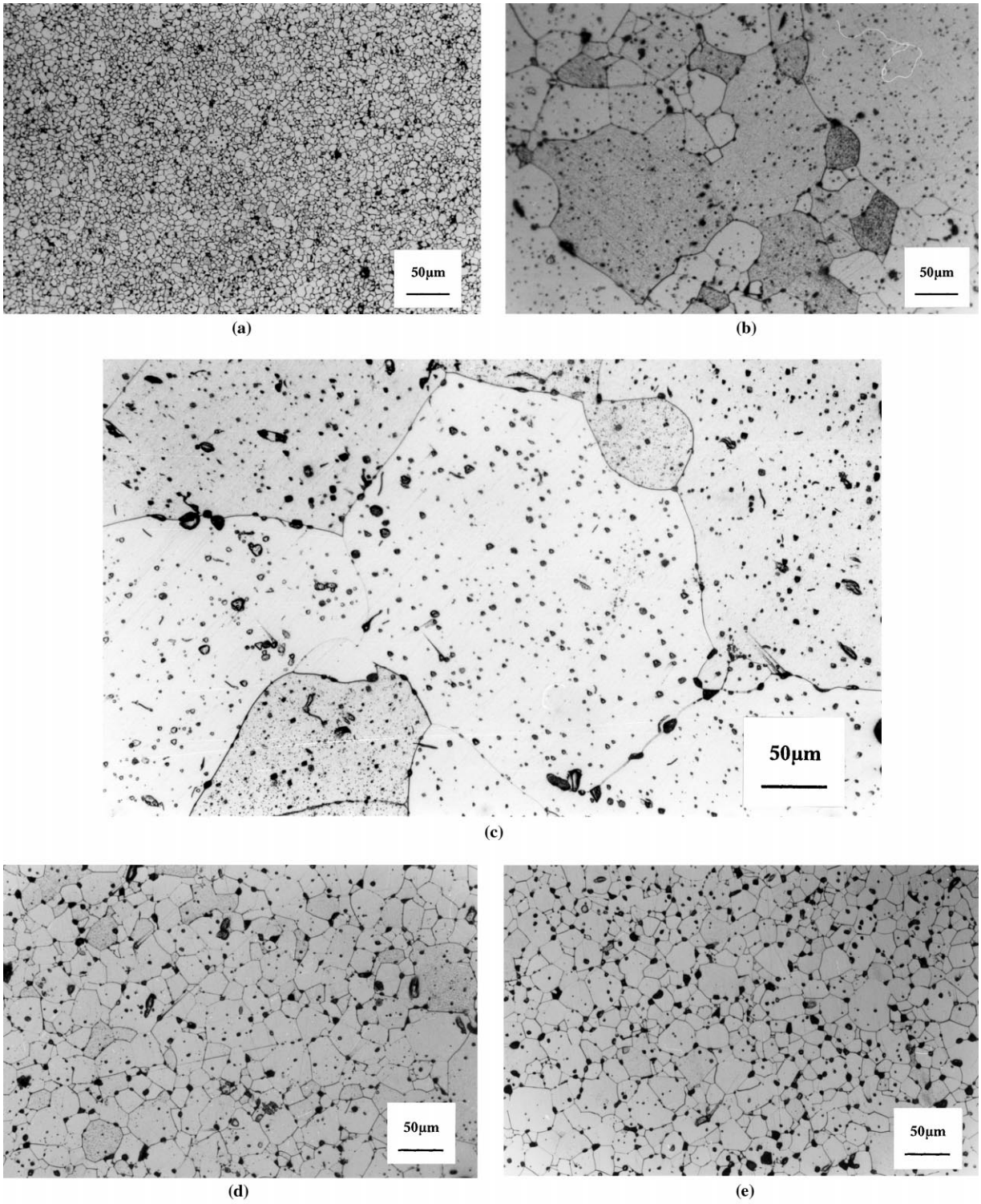

Fig. 2. Typical optical micrographs of Mn–Zn ferrites undoped and doped with B_2O_3: (a) undoped (boron-free); (b) 0.10 wt.% B_2O_3; (c) 0.15 wt.% B_2O_3; (d) 0.25 wt.% B_2O_3; (e) 0.5 wt.% B_2O_3.

doping level, a relatively uniform microstructure with large grain size (39.5±3.3 μm) was obtained (Fig. 2d). Beyond this doping level the average grain size gradually decreases with further increase of B_2O_3 content (Fig. 2e, 0.5 wt.%). The average grain size as the function of B_2O_3 additions is shown in Fig. 3.

After calcination and deagglomeration, the particles of the ferrite powder are fine crystallites. The average particle size is approximately 0.2 μm. which is a good agreement with the particle size of 0.15 μm reported by Rozman et al.[19] on the citrate-gel derived Mn–Zn ferrites. During gel processing and precursor calcination the added boric acid transformed into vitreous state boric oxide. This semi-ordered vitreous boric oxide consists of a network of trigonal BO_3 units in which the six-membered boronxin ring predominated.[20] On the assumptions that the ferrite crystallites can be approximated to spheres and the vitreous B_2O_3 covers these crystallites, calculation of surface areas based on the different crystallite sizes enables that the critical coverage by B_2O_3 to be assessed. If the bond distance (B–O) is taken as 1.30 Å,[20] the diameters of B^{3+} and O^{2-} are 0.23 and 1.32 Å, respectively,[21] then the covering area of a basic six-membered boronxin ring is approximately 4.15×10^{-15} cm^2. Fig. 4 shows the relationship between B_2O_3 doping level and the surface area of the calcined particles covered by such a ring arrangement. If 0.20±0.02 μm is taken as the powder particle size, the relationship between the small B_2O_3 doping level and the atomic covering-layer on the powder particles is shown in Fig. 5.

Due to the low melting temperature of B_2O_3 (460°C), it is anticipated that liquid phase sintering occurred during sintering,[4] which promoted the rapid grain growth. When the doping level is low, the powder particles are likely to be covered by only a single layer of B_2O_3, which appears to be insufficient to allow homogeneous liquid sintering. Additionally, as the liquid phase appears to preferentially fill the triple points between the solid particles (see Fig. 6), the amount of intergranular liquid phase will be reduced . Hence discontinuous grain growth occurs and a duplex microstructure is formed. This rapid increase in grain growth leads to the most pores being trapped within the exaggerated grains, as shown in Fig. 2b and c. The average grain size of such duplex structure can not be determined by Mendelson methods,[18] (the doping levels at which the discontinuous grain growth occur is indicated in Fig. 3). As the B_2O_3 doping level increases to 0.25 wt.%, the doping amount is theoretically equivalent to 2–4 atomic layers to cover the powder particles. Thus the discontinuous grain growth disappears and a relatively uniform microstructure is obtained. Sale and Albiston[22] have reported that the 2–4 atomic layer coverage is

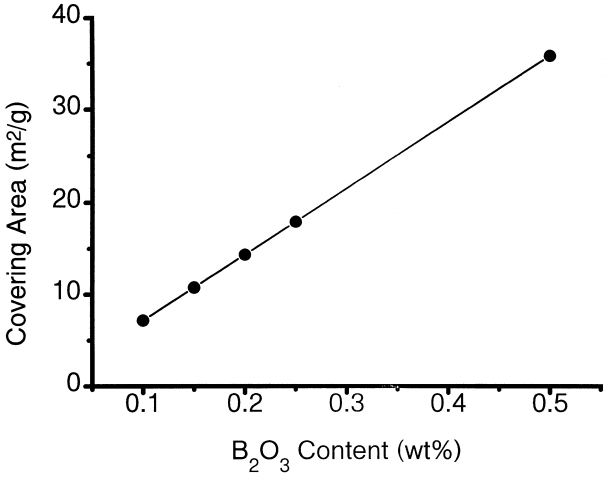

Fig. 4. The relationship between the covering area and the B_2O_3 content.

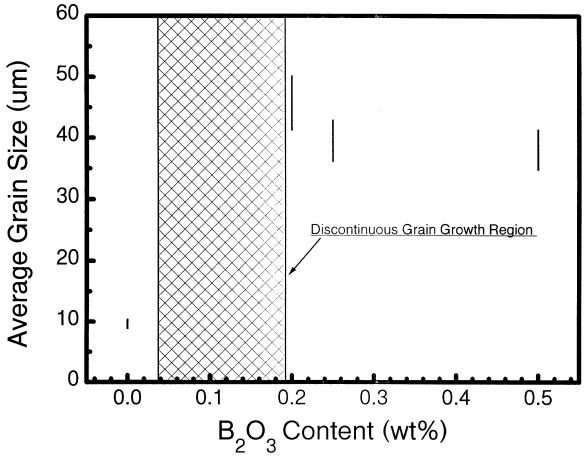

Fig. 3. The relationship between average grain size and the B_2O_3 content.

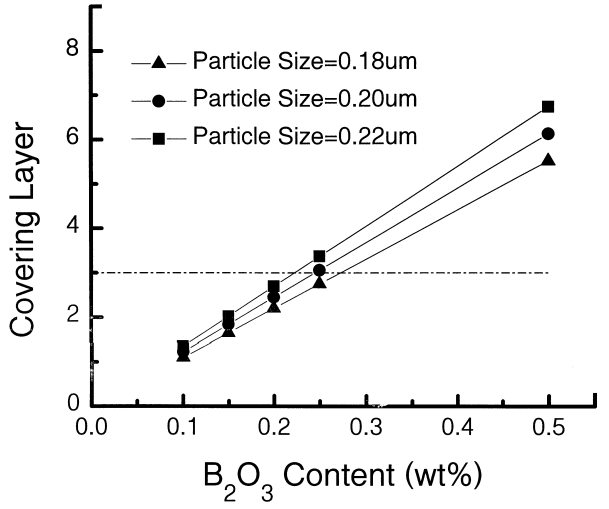

Fig. 5. The relationship between the covering layer and the small B_2O_3 doping levels.

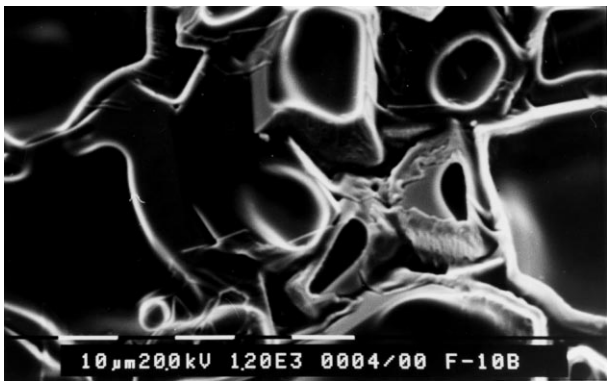

Fig. 6. Typical SEM photograph which shows the triple points between the grains are preferentially filled by B-liquid phase.

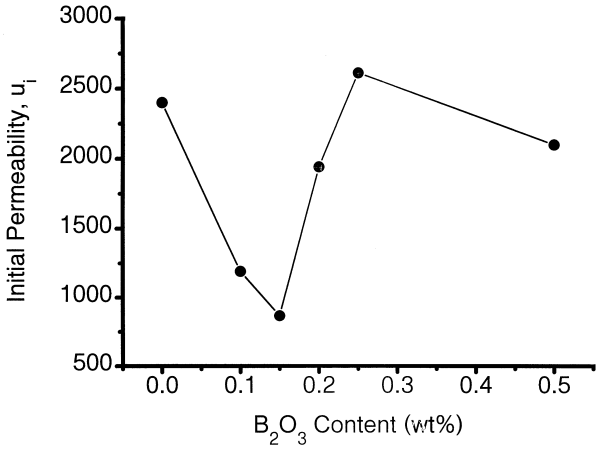

Fig. 7. Variation of the initial permeability (μ_i) and B_2O_3 content for Mn–Zn ferrites.

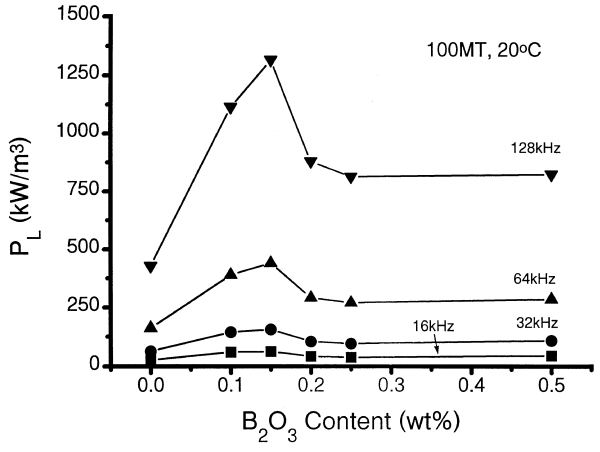

Fig. 8. Variation of the power loss (P_L) and B_2O_3 content for Mn–Zn ferrites.

essential for the activated sintering in Ag–W composite powder doped with Ni, therefore, 2–4 atomic layer coverage could be the critical to effective sintering for other powders doped with small amount covering dopants. With further increases in the B_2O_3 content, the increased liquid phase enables more uniform grain growth, which results in a microstructure with much less intragranular pores, but the intergranular pores become larger during sintering. Beyond the 0.25 wt.% B_2O_3 doping level, the increased grain boundary phase and intergranular pores appear to impede the grain growth. Therefore the average grain size gradually decreases, and the porosity increases. The mechanism for impeding grain growth by the increased B_2O_3 liquid phase is not quite clear, but it must be related to the increased intergranular pores and the longer diffusion paths (due to the thicker grain boundary phase) which may slow down the mass diffusion through liquid phase. The increased porosity is related to the loss of B_2O_3 at high sintering temperature.[20]

3.2. Initial permeability (μ_i) and power loss (P_L)

The variation of initial permeability (μ_i) as a function of B_2O_3 content is plotted in Fig. 7. The initial permeability (μ_i) of the undoped sample is about 2400. It decreases sharply with small amounts of B_2O_3 additions (0.1 and 0.15 wt.%). Further increasing the B_2O_3 doping level, the μ_i value recovers and reaches the maximum value (~2600) at 0.25 wt.% doping level, which is slightly higher than that of undoped samples. Beyond 0.25 wt.% doping level the initial permeability decreases again with further increases in B_2O_3 content.

Fig. 8 shows the relationship between power loss (P_L) and the B_2O_3 doping level. The undoped samples have the lowest values of power loss at all measuring frequencies. The power loss (P_L) increases rapidly at small doping levels (0.1–0.15 wt.%), then shows a second minimum value at 0.25 wt.% doping level. With further additions of B_2O_3, the P_L value increases again.

Comparing Fig. 7 and Fig. 8, it is obvious that the trend of the variation of power loss is almost the complete opposite of the changes in the initial permeability. It is well known that different microstructures (such as grain size, uniformity, porosity and second phases) influence strongly the magnetic properties of the ferrite materials. These changes in the magnetic properties for these ferrites doped with B_2O_3 are closely related to the observed microstructures. Generally, a large grain size is favourable for higher initial permeability and small grains are desired for lower power loss.[23] However, intragranular pores may pin, or impede the movements of, domain walls which leads to deteriorate magnetic properties.[24] The low initial permeabilities and high power losses determined for the samples doped with 0.1–0.15 wt.% B_2O_3 are attributed to their duplex microstructures. At 0.25 wt.% doping level, the larger grain size should give the much higher value of the initial permeability (μ_i) than that of the undoped samples.

However, as seen in Fig. 2d there are some intragranular pores in the grains and the distance between the pores all important as these intragranular pores pin domain walls. In addition, the larger grain size results in an increase in the power loss. As a result, these samples containing 0.25 wt.% B_2O_3 have slightly higher μ_i values than that of the undoped samples, but possess higher power loss. With higher B_2O_3 doping levels the increased porosities and B-rich phase are felt to be responsible for the deteriorated magnetic properties.

3.3. Impedance analysis

Fig. 9 shows the impedance measurements, which are related to changes in microstructure that result from the B_2O_3 additions. The complex–impedance dispersion curve of the undoped sample (which has small and uniform average grain size) is in the form of a large semi-circle. Compared to the data for the undoped sample, the impedance results for the samples doped with small amounts B_2O_3 (0.1 and 0.15 wt.%) show quite small semi-circles, which may be a result of their giant grain sizes. The resistances of sample R^{∞} (at frequency, $f=\infty$) and R^0 (at frequency, $f=0$) were determined from the intercepts of the complex–impedance dispersion curve with the real impedance (Z') axis. The data for R^{∞} and R^0 are given in the middle columns of Table 1.

Several models[25–27] have been reported to be used for interpreting the results of impedance measurement on soft ferrites. Amongst them the Koops' model[25] is a classical model. The idealized microstructure for the Koops' model assumes that the ferrite is a grain structured conductor in which layers of poorly conducting grain boundary material separates the grains. The Koops's model considers the effects of dielectric constant ($\epsilon=\epsilon_0\epsilon_r$, where ϵ_0 and ϵ_r are vacuum dielectric constant and relative dielectric constant, respectively) and the thickness ratio (χ) between grain boundary layers and bulk materials. The simplified equivalent circuit of the Koops' model is shown in Fig. 10. Based on this equivalent circuit, Koops reasonably assumed the dielectric constants for both grain and grain boundary materials are same,[25] such that the relationship between the measured resistivity ρ_p, bulk resistivity ρ_b and grain boundary resistivity ρ_{gb} could be simply described by the following equation:[25]

$$\rho_p = \rho_b + \frac{\chi\rho_{gb}}{1 + 4\pi^2 f^2 \varepsilon_o^2 \varepsilon_r^2 \dfrac{\rho_{gb}^2 \rho_b}{\chi\rho_{gb} + \rho_b}} \quad (1)$$

which means the measured value ρ_p is the function of ρ_b, ρ_{gb}, χ, ϵ_r and f (frequency). Here, f is known and bulk resistivity ρ_b can be estimated (assuming at $f=\infty$, the R^{∞} is determined by ρ_b). Therefore, if the values of χ and ϵ_r can be determined, then to find the value of ρ_{gb} which can be derived from the best fit of the curve of $\rho_p \sim f$.

The TEM observation and the measurements on the undoped sample reveals that the thickness of intrinsic grain boundary is about 10 nm. Based on the results of

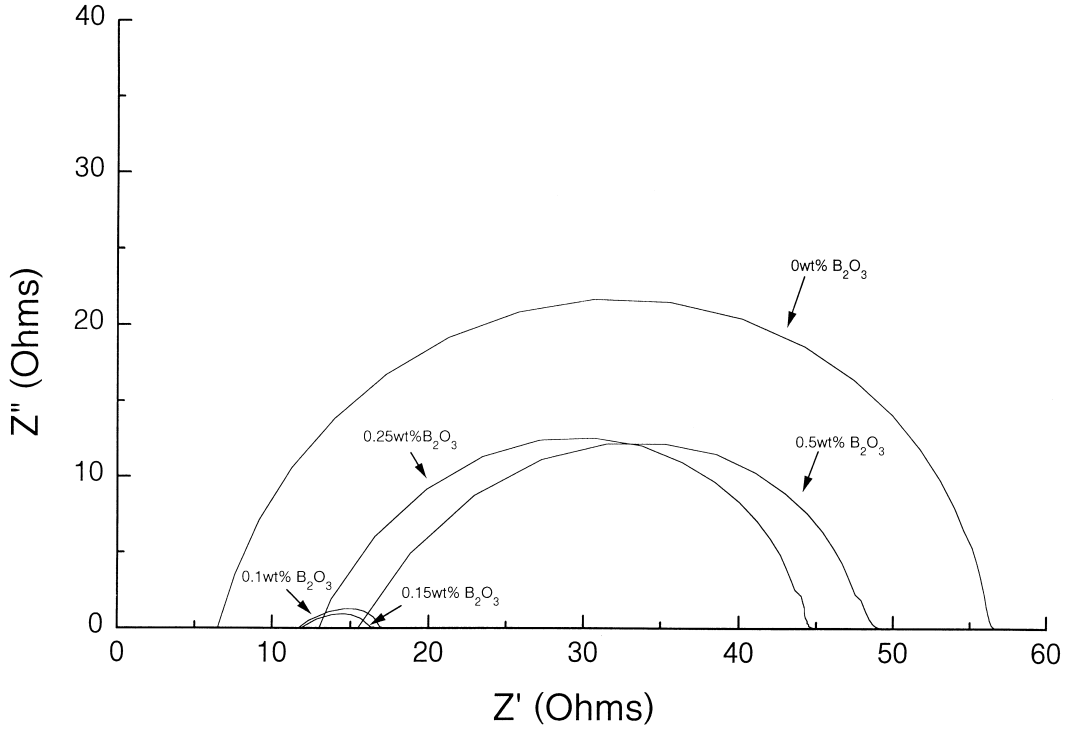

Fig. 9. The results of impedance measurement for Mn–Zn ferrites doped with B_2O_3.

Table 1
Impedance results

B_2O_3 doping level (wt.%)	Thickness of grain boundary (nm)	Number of cross grain boundary	Total thickness of grain boundaries[a] (nm)	Ratio χ	R^{∞} (Ω)	R^{0} (Ω)	R_{gb} (Ω)	ρ_b (Ω·m)	ρ_{gb} (Ω m)	
									Simple model	Koops' model[b]
0	10	313	3.13×10^{-3}	1.04×10^{-3}	6.5	56.7	50.2	0.11	844	793
0.1	11	~20	2.02×10^{-4}	7.33×10^{-5}	11.7	17.3	5.7	0.20	1340	1342
0.15	11.5	~15	1.73×10^{-4}	5.75×10^{-5}	11.6	17.2	5.6	0.20	1600	1566
0.25	12	76	9.12×10^{-4}	3.04×10^{-4}	13.0	43.9	30.9	0.22	1720	1766
0.50	12.5	79	9.88×10^{-4}	3.29×10^{-4}	15.4	49.4	34.0	0.26	1720	1668

[a] Assuming the thickness of intrinsic grain boundary interface is 10 nm.
[b] For Koops' model using $\epsilon_r = 20$. (Ref.: Koops' paper).

TEM and the average grain size measurements, the estimated thicknesses of samples and numbers of cross grain boundary are listed in Table 1. Therefore, the ratio χ between grain boundary layer and bulk materials can be calculated. By assuming the relative electric constant ϵ_r of ferrite materials is 20,[25] the grain boundary resistivities ρ_{gb} calculated for the samples are shown in the last column in Table 1. The resistivity–frequency relationships for experimental data and the calculated data, using Koops' theory, are shown in Fig. 11, where it can be seen that the calculated data fit the experimental data quite well.

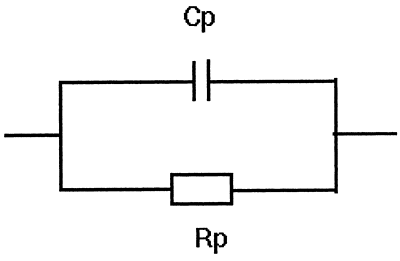

Fig. 10. The equivalent circuit of Koops' model.

To discuss further the data, a simple model has been proposed. This model is derived from the brick wall model, where the grains have the shape of cubes with dimension D and it is assumed that the total thicknesses of the intrinsic grain boundary interface and the B_2O_3-rich phase can be estimated by TEM observation. The equivalent circuit for the combination of individual circuits

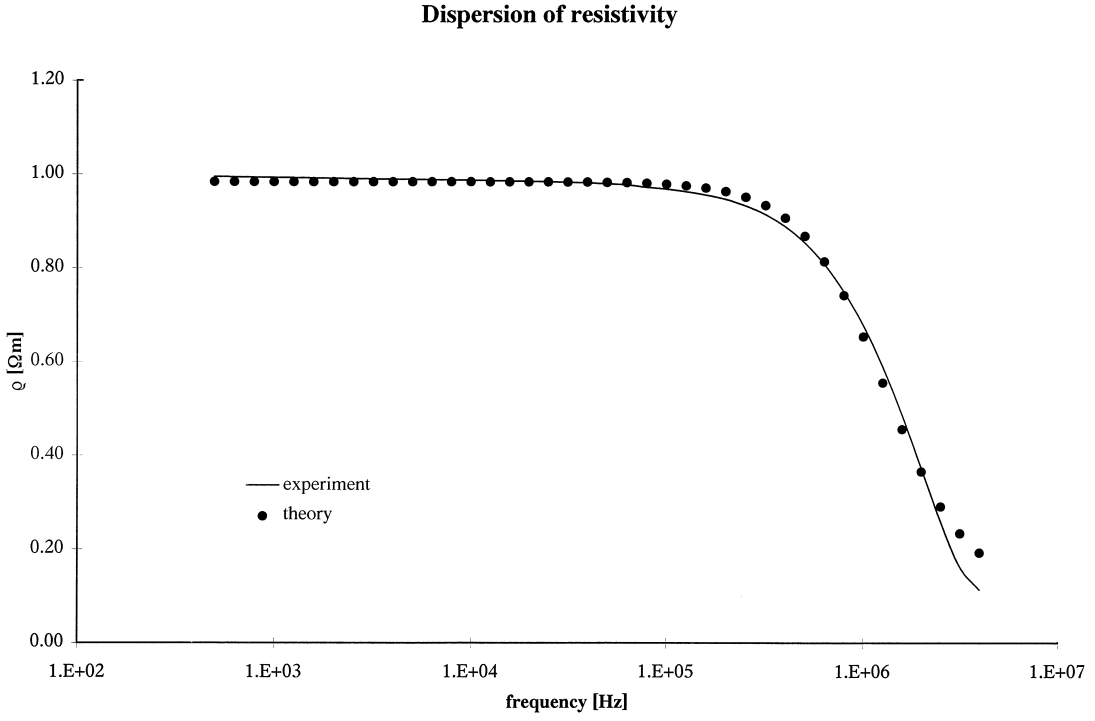

Fig. 11. The typical dispersion of resistivity.

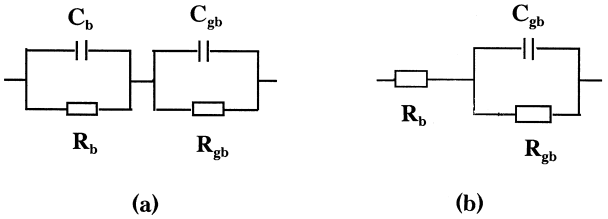

Fig. 12. The equivalent circuit of simple model.

can described as two circuits connected in series, as shown in Fig. 12a, where R_b and C_b related to the bulk material and R_{gb}, C_{gb} related to the grain boundary phase. Since in soft ferrites the bulk resistance is much lower than the grain boundary resistance and the bulk capacitance is negligibly small, the equivalent circuit can be simplified as Fig. 12b. At $f=\infty$, R^{∞} can be treated as R_b, such that R_{gb} can be obtained by using Eq. (2):

$$R^0 = R_{gb} + R_b \tag{2}$$

By using the obtained values of R_b and the average grain sizes, the simple model can be used to estimate the grain boundary resistivities of the samples. The estimated ρ_{gb} values obtained for the samples by this simple model are also shown in Table 1. They are good agreement with those obtained from Koops' model.

From the results of impedance analysis, it can be shown that B_2O_3 doping increases the grain boundary resistivity, since B_2O_3 segregates to grain boundary and the B_2O_3-rich phase that is produced promoted the grain growth. However, from the power loss results reported in Section 3.2, it can be seen that the increased resistivity of the boundaries did not decrease the power loss for the samples doped with B_2O_3. This is because of the much large grain size and the increased porosity obtained on those samples, as the eddy current loss is proportional to the square of the average grain size and the reciprocal of resistivity.

Furthermore, whilst B_2O_3 has previously been considered to act as only a grain boundary additive, the impedance analysis indicates that the bulk resistivity is also increased relative to undoped materials, thus implying the possible solution of some B_2O_3 within the ferrite spinel structure or an effective change in composition of the grains as a results of the presence of B_2O_3 at the grain boundaries. A further investigation will be carried out to resolve this.

4. Conclusion

1. The presence of B_2O_3 promotes significantly grain growth in iron-excess Mn–Zn ferrites, but B_2O_3 does not benefit the magnetic properties of these ferrites. At low doping levels (<0.2 wt.%), discontinuous grain growth occurs, which results in a duplex microstructure that is responsible for the poor magnetic properties obtained at these doping levels. Comparison with undoped samples shows that a slightly higher value in the initial permeability and a second minimum value in power loss are obtained for the samples doped with 0.25 wt.% B_2O_3, which shows a relatively uniform microstructure with large grain size. Further increasing the B_2O_3 doping level, gave the increased porosity and B-rich phase which result in the deteriorated magnetic properties.
2. The impedance analysis indicates that both bulk resistivity and grain boundary resistivity are increased as B_2O_3 is added to the ferrite, which implies the possible solution of some B_2O_3 within the spinel or an effective change in composition of the grains as a result of the presence of B_2O_3 at the grain boundaries.
3. Both Koops model and the proposed simple model can be successfully used in the impedance analysis of Mn–Zn ferrites. The microstructural information obtained from both SEM and TEM are important in the interpretation of those impedance results.

Acknowledgements

The authors would like to acknowledge the financial support of EPSRC which has made possible the research work reported here.

References

1. Snelling, E. C., *Soft Ferrites-Properties and Applications*, 2nd edn. Butterworth, London, 1988, p. 19.
2. Goldman, A., *Modern Ferrite Technology*. Van Nostrand Reinhold, New York, 1990, p. 87.
3. Stijntjes, T. G. W. et al., *Proc. ICF-1*, Tokyo, Japan, 1970, p. 194.
4. Neijts, R. C., *Philips Report*, TR-245-268, 1988, p. 15.
5. Stuijts, A. L., *Proc. Brit. Ceram. Soc.*, 1964, **2**, 73.
6. Fan, J. and Sale, F. R., Influnce of B_2O_3 on the production of pure, gel-processed Mn-Zn ferrites. *J. Phys. IV*, 1997, **7**, 81–82.
7. Takeda, T. and Kiyama, M., *Proc. ICF-1*, Tokyo, Japan, p. 69, 1970.
8. Sako, T., Kuroda, C. and Saito, M., *Proc. ICF-1*, Tokyo, Japan, p. 72, 1970.
9. Marcilly, C., Courty, P. and Delmon, B., *J. Am. Ceram. Soc.*, 1970, **53**, 56.
10. Courty, P., Ajot, H., Marcilly, C. and Delmon, B., *Powder Technol.*, 1973, **7**, 21.
11. Anderton, D. J. and Sale, F. R., *Powder Metall.*, 1979, **22**, 14.
12. Sale, F. R. and Mahloojchi, F., Citrate gel processing of oxide superconductors. *Ceram. Int.*, 1988, **14**, 229–237.
13. Fan, J. and Sale, F. R., Citrate gel route processing of ZnO varistors. *Brit. Ceram. Proc.*, 1994, **52**, 151–157.
14. Mahloojchi, F. and Sale, F. R., *Ceram. Int.*, 1989, **15**, 51.
15. Chien, Y.-T. and Sale, F. R. Microstructureal development and magnetic properties of vanadium pentoxide doped, gel-derived Mg–Mn–Zn ferrite. *Proc. ICF-6*, Tokyo, Japan, 1992, pp. 301–304.

16. Sale, F. R., Fan, J. and Chien, Y.-T., The effects of V_2O_5 on the microstructure and magnetic properties of gel-derived Mg–Mn–Zn and Mn–Zn ferrites. *Am. Ceram. Trans*., 1995, **47**, 155–167.
17. Fan, J. and Sale, F. R., Analysis of power loss on Mn–Zn ferrites prepared by different processing routes. *IEEE Trans. Magnetics*, 1996, **32**, 4854–4856.
18. Mendelson, M. I., *J. Am. Ceram. Soc*., 1969, **52**, 443.
19. Rozman, M., Drofenik, M. and Kolar, D., *Proc. Third Euro-Ceramic Conference*, ed. P. Duran and J. F. Fernandez. Spain, vol. 1, 1993, p. 341
20. Nies, N. P. and Campbell, G. W., Chapter 3. In *Boron, Metallooron Compounds and Boranes*, ed. R. M. Adams. Interscience Publishers, New York, 1964, pp. 55.
21. CRC, *Handbook of Physics and Chemistry*, 70th edn. Boca Raton, Florida, 1989–90, F-187.
22. Sale, F. R., Albiston, J. N., Production and sintering of Ag–W composites containing Ni. In *Modern Developments in Powder Metallurgy*, vol. 19, compiled by P. U. Gumneson and D. A. Gustafson. American Powder Metallurgy Institute, New Jersey, 1988, pp. 75–89.
23. Goldman, A., *Modern Ferrite Technology*. Van Nostrand Reinhold, New York, 1990, pp. 115–144.
24. Guillaud, C., Villers, G., Marais, A. and Paulus, M., *Solid State Physics in Electronics and Telecommunications*, vol. 3, London, Academic Press, 1960. p. 71.
25. Koops, C. G., On the dispersion of resistivity and dielectric constant of some semiconductors at audiofrequencies. *Physical Review*, 1951, **83**, 121–124.
26. Cheng, H.-F., Modeling of electrical response for semiconducting ferrite. *J. Appl. Phys*., 1984, **56**, 1831–1837.
27. Drofenik, M., Znidarsic, A. and Makovec, D., Influence of the addition of Bi_2O_3 on the grain growth and magnetic permeability of MnZn ferrites. *J. Am. Ceram. Soc*., 1998, **81**, 2841–2848.